Fundamental J. Mathematical Physics, Vol. 1, Issue 2, 2011, Pages 69-98
Published online at http://www.frdint.com/

SIMULATION OF MUONIC CATALYZED FUSION USING THE MONTE-CARLO METHOD

ALIREZA HEIDARI[a], SEYEDALI VEDAD[a], O. ANWAR BÉG[b] and MOHAMMADALI GHORBANI[a,*]

[a]Institute for Advanced Studies
Tehran 14456-63543, Iran
e-mail: mohammadalighorbani1983@yahoo.com

[b]Multi-Physics Simulation, Aerospace Engineering
Mechanical Engineering Subject Group
Department of Engineering and Mathematics
Sheffield Hallam University
Sheaf Building, Sheffield
S1 1WB, UK

Abstract

The μCF (muonic catalyzed fusion) cycle is investigated using Monte-Carlo simulation. This simulation starts when a muon enters the deuterium-tritium mixture. We use the cross-sections of the processes which arise in the μCF cycle, which is the same process as that which the muonic atoms experience in their frequent collisions. To simulate the dynamic process, a numerical code based on Monte-Carlo simulation has been developed. This code also features a time parameter in order to enable computation of the time spectrum for different events, which occur when the μCF cycle is reached. Additionally the time spectrum for neutrons resulting from fusion is evaluated. Furthermore, the energy

Keywords and phrases: fusion neutrons, time spectrum, muonic atoms, energy spectrum, muonic catalyzed fusion, Monte-Carlo simulation, quantum engineering, fusion yield, cycle rate, total sticking coefficient.

*Corresponding author

Received December 31, 2011

spectrum of the muonic atoms is calculated at different times and these results are depicted graphically. It is feasible to determine the fusion yield (χ), the cycle rate (λ_c) and, also, the total sticking coefficient (W) in different hydrogen isotopic concentration conditions using the Monte-Carlo computations. To validate the present computations, results are compared with alternative computational methods and also experimental data.

1. Introduction

Muonic catalyzed fusion cycle research (μCF) has stimulated considerable theoretical, practical and computational research in the quantum engineering and physics research community [1-3]. μCF cycle computations based on experimental data, are generally conducted based on process rates, and this has been shown to greatly assist μCF experimental investigations. Computational modeling in this regard, in particular featuring cycle cinematic solution methods [4] and the Monte-Carlo method [5, 6] has demonstrated considerable success. In the cycle cinematic solution, one differential equation system which describes the chain processes in μCF cycles must, at first, be written for the particles population involved in the cycle and, subsequently be solved. However, it is important to emphasize that the cinematic equations are written in thermal equilibrium conditions [3, 4]. Also, different processes cause the creation of energetic muonic atoms, the kinetic energies of which are in excess of the average thermal energy of the medium particles [6]. The Coulomb de-excitation, muonic isotopic transition, and spin inversion are examples of important processes which create super-heating atoms. The formation of muonic molecules which have important roles in the muonic catalyzed fusion is largely influenced by the kinetic energy of muonic atoms [7]. In the cycle cinematic solution under thermal equilibrium conditions, the rate of the muonic molecule formation and other processes which occur in the μCF cycle are in fact an averaging of the process rate on the kinetic energy distribution of the muonic atoms which are computed on the basis of the Maxwellian distribution [8]. Therefore, under these conditions, the energy dependence of processes in the μCF cycle, especially the formation of $dt\mu$ molecules by super-heating $t\mu$ atoms, is ignored.

As far as Monte-Carlo simulation is concerned, μCF cycle investigation is a prominent area of application. In this article, the muonic catalyzed reactions cycle is simulated using this statistical method. Employing Monte Carlo simulation enables

computations which are closer to the real conditions which arise in the μCF cycle. This simulation starts when a muon enters the deuterium-tritium mixture. By utilizing the cross-sections of the processes which occur in the μCF cycle, the same process is pursued as arises when the muonic atoms engage in frequent collisions. Finally, when a muon sticks to the charged particles generated by fusion, or when it decays slowly, this muon reaches the end of its path and a subsequent simulation is initiated for the next muon. To achieve this computationally, we employ a robust computer code programmed in FORTRAN. The temporal parameter is also featured in the program enabling the computation of time spectra for different events which occur in the μCF cycle. In other words, the number of chain events in the μCF cycle is determined systematically at each time interval. Also, the time spectra for neutrons generated by fusion are evaluated. Employing the time parameter permits a much more rigorous and complete analysis of the events which characterize the μCF process. The energy spectrum of muonic atoms is calculated at different times and visualized graphically. Furthermore, we can determine the fusion yield χ (the number of fusions for each muon), the cycle rate χ (the reverse average time of cycle passage from the time of muons' entrance till the fusion time) and, also, the total sticking coefficient W (the total probability of muon's sticking to the diffusion-resulted charged products) in different hydrogen isotopic concentration conditions using the Monte-Carlo computation. Our results are compared with different other methods' computations and excellent correlation is achieved.

2. The Muonic Atoms Collision Processes in D / T Mixture

To simulate the μCF cycle correctly requires a comprehensive understanding of the collision processes of muons and muonic atoms with medium particles and an accurate evaluation of their cross-sections. It is worth noting that a muon is moderated while entering an area in hydrogen isotopes. The source of a muon in the muonic catalyzed fusion cycle can be either:

(1) Paion decay which is caused by the collision of the light nucleus with high energy in accelerators. The estimated energy for these muons is about 4.3 MeV.

(2) Muons which become free as a result of fusion, with an estimated energy of about 10 keV [1].

The muons of both of these sources must be moderated to become capable of

capturing and forming a muonic atom. The important recognized processes involved in slowing down the muons are the non-elastic collisions with medium atoms and ionization, which immediately moderate the muons energy [1]. Subsequently a muon is immediately trapped in the $d\mu$ and $t\mu$ muonic atoms in the very excited levels. Generally the number of the related level is in excess of the quantum number $n = 14$ [9, 10]. After an interval of about (10^{-11}s), these atoms reach a ground state [9, 11]. During the process of transitions to the ground state the radiative, the external Auger effect, and the Coulomb transition take place [8-12]. The continuous moderating process of slowing down of muonic atom in the medium is also generated by elastic collisions. It is evident that all of these processes are involved in a competition and, depending on the environmental conditions, there is the probability of changing their rates. In other words, their relative importance depends on the physical conditions which include the medium density and hydrogen isotope concentration. One must note that the de-excitation rates are about (10^{-11}s) which are 10^2 times more than the thermal rate of muonic atoms in the ground state, $\lambda_{\text{th}} \approx 10^9 \phi \text{s}^{-1}$, in which ϕ is the medium density on the basis of liquid hydrogen density $(\phi = N/N_\circ,\ N_\circ = 4.25\times10^{22}\text{cm}^{-3})$ [1]. Owing to the fact that the thermal process for muonic atoms in excited states happens with a higher velocity compared to the ground states $\lambda_{\text{th}}^{ex} \approx 1.5\times10^{12}\text{s}^{-1}$; therefore, a great quantity of the muonic atoms which are formed in the ground state are super-heating. In addition, owing to the excited states, immediately becoming thermal, their energy distribution is relatively close to the Maxwellian distribution. Additionally also, because of the complexities present in the transition processes, some of which cause the creation of super-heating atoms and the others moderate the kinetic energy, and also their rates are a function of kinetic energy, one cannot determine the muonic atoms' initial energy distribution with great precision [6]. However, usually in analysis, the Maxwellian form around the super-heating energies is considered for the muonic atoms' initial energy distribution. The same approximation is, also, used in this article.

The muonic atoms collision processes in a binary mixture which must be simulated are:

(1) Elastic dispersion

$$(x\mu)_n + d,\ t \rightarrow (x\mu)_n + d,\ t \tag{1}$$

$$(x\mu)_n + D, T \rightarrow (x\mu)_n + D, T \tag{2}$$

$$(x\mu)_n + D_2, T_2 \rightarrow (x\mu)_n + D_2, T_2 \tag{3}$$

in which n is the principal quantum number and x reads d or t .

(2) Isotopic transition

$$(d\mu)_n + t \rightarrow (t\mu)_n + d + \frac{48}{n^2}\,\text{eV}. \tag{4}$$

(3) Ultra-small transitions

(a) Spin-flip caused by symmetric collisions:

$$d\mu\uparrow\uparrow + d \rightarrow d\mu\uparrow\downarrow + d + 0.049\,\text{eV}, \tag{5}$$

$$t\mu\uparrow\uparrow + t \rightarrow t\mu\uparrow\downarrow + t + 0.24\,\text{eV}. \tag{6}$$

(b) Spin-flip caused by non-symmetric collisions:

$$d\mu\uparrow\uparrow + t \rightarrow d\mu\uparrow\downarrow + t, \tag{7}$$

$$t\mu\uparrow\uparrow + d \rightarrow t\mu\uparrow\downarrow + d. \tag{8}$$

(4) Muonic molecule formation in resonance and non-resonance form:

$$d\mu + DA \rightarrow [(dd\,\mu)aee], \quad (A = D \text{ or } T;\ a = d \text{ or } t), \tag{9}$$

$$t\mu + DA \rightarrow [(dt\mu)\,aee], \quad (A = D \text{ or } T;\ a = d \text{ or } t). \tag{10}$$

It is clear that isotopic transition creates quick muonic atoms and the ultra-small transition, also, causes an increase in the energy of muonic atoms. Also, elastic collisions moderate their kinetic energy. Consequently, in muonic atoms collisions and heating process, there is the probability of muonic molecules which can be formed in resonant form [1, 13].

The muonic molecules formation, to a great extent, depends on the collision energy. The muonic atoms' spin is, also, effective in the molecule formation rate. The reactions rate [i.e., equations (9) and (10)] is computed in different spins states in the binary mixture, as a function of the $t\mu$ atom's kinetic energy, by Feinmann-Panomarov approach [13]. Usually, the molecule formation average rate is reached by the Maxwellian distribution approximation of the $t\mu$ atoms kinetic energy:

$$\lambda^{F}_{dt\mu}(T) = \int_{0}^{\infty} \lambda^{F}_{dt\mu-x}(E) f(E, T)\, dE,$$

$$f(E, T) = 2\left(\frac{E}{\pi}\right)^{\frac{1}{2}} T^{\frac{3}{2}} \exp\left(\frac{-E}{kT}\right) \tag{11}$$

in which F denotes the spin state of the $t\mu$ atom, T is the medium temperature, and x reads either d or t. In this computation, it is assumed that, at first, the muonic atom reaches a thermal equilibrium with the medium and, in due course, a muonic molecule is formed. In fact, in computations related to the cycle cinematic method, the use of this approximation is inevitable. However, as mentioned before, the muonic atoms in their ground state are not necessarily in thermal equilibrium with the medium. Since in the present article, in each stage, the muonic atom's energy is computed and the collision processes' cross-sections, (which are function of the energy), are implemented, the computations possess higher precision.

To execute this simulation, at first, the need for determining the cross-sections of processes (1 to 10) is imperative. The cross-sections of these processes as used in the present study article were, previously, calculated by the Adamczak [14]. As discussed earlier, the different reaction cross-sections of the muonic atoms in collision with atoms and medium molecules are energy functions and in each collision, the muonic atom's energy must be determined after the collision so that one can follow the collision reactions process using cross-sections.

In energies higher than 1eV, one can assume the muonic atoms direct collision with nucleus targets [15-17] and ignore electron screening effects. The molecule formation cross-sections are, also computable from the molecule formation rate, $\lambda_{ij\mu}$, which can be achieved easily [13]:

$$\lambda_{ij\mu} = \sigma_{ij\mu}(E)\, vN \tag{12}$$

in which $\lambda_{ij\mu}$ and $\sigma_{ij\mu}$ are the rate and cross-section of $ij\mu$ molecule formation, respectively. Also, v is the muonic atom velocity and N the medium atomic density.

3. Monte-Carlo Simulation

If one could, from the very beginning of muon's entrance to D/T mixture, in a

computer program, using the Monte-Carlo method, follow step-by-step all of the processes which happen (as elaborated in the previous section) it would then be possible to achieve more realistic conditions in the muonic catalyzed fusion. To accomplish this, in this article, an algorithm is provided in the computer code developed.

When a muon enters the D/T medium, it is immediately absorbed in the highly excited states of the munoic atoms, on the basis of the de-excitation processes explained in Section 2, and transits into the lower states. Owing to the fact that the de-excitation processes occur much faster than the other processes in the μCF cycle, in the present investigation simulation starts when the muonic atoms reach the ground state. Furthermore the de-excitation processes effects are mimicked by applying the muonic atom kinetic energy distribution in its ground state. The latter depends on the de-excitation process and, also, incorporates the parameter q_{1s} which represents the probability of $d\mu$ atom's reaching the ground state. Since from $d\mu$ atom's excited states, a muon is transited to tritium with a higher velocity, it is probable that before $d\mu$ atom's reach the ground state, the muon is transited to tritium.

In this program, at first, hydrogen isotope concentrations are chosen in the D/T mixture (c_d and c_t). Next considering the fact that we aim to repeat this numerical computation for so many munos (for instance 10^6 particles) and due to the averaging from the results, one counter is determined which ranks a place for itself in the muon. Based on the determined isotopic concentration, the probability of collision between muon and deuteriums and tritiums are different. Creating a random number (r_1) and comparing it with c_d and c_t concentration, assuming that $c_d + c_t = 1$, one can determine the type of muonic atom to be formed. In other words, if $r_1 \le c_t$, the collision will be with tritium or deuterium. From now on, similar processes will happen based on the formation of $d\mu$ or $t\mu$. For instance, now, the canal related to $t\mu$ collisions process, which is more important, is explained.

As explained in Section 2, $t\mu$ atom can have different collisions with medium particles (hydrogen isotope molecules and atoms), the cross-sections of some of which, (e.g., non-elastic collision or spin-flip and molecule formation), depend on the atom spin (F), which is either 1 or 0. Therefore, initially the $t\mu$ atom spin must be determined. Considering the statistical weight of the $t\mu$ atom spin states $(2F + 1)$,

for $F = 1$, there exist three states and for $F = 0$, there is only one state. Consequently, $t\mu$ atoms are formed with probabilities of $\frac{3}{4}$ and $\frac{1}{4}$ with $F = 1$ and $F = 0$ spins, respectively. Creating a random number (r_2) and comparing it with these probabilities, one can determine the muonic atom spin state.

Since in the D/T medium, there exist D_2, DT and T_2 molecules, the next stage is determining the type of molecule with which the atom $t\mu$ collides. The ratio of their concentrations, based on the atomic concentrations, equals $c_d^2 : 2c_d c_t : c_t^2$. Since we have $c_d^2 + 2c_d c_t + c_t^2 = 1$, one can determine the type of molecule collided with by creating the random number (r_3) and comparing it with $c_d^2,\ 2c_d c_t,\ c_t^2$.

Owing to the fact that the $dt\mu$ molecule is formed in a resonant form and a higher rate compared to other muonic molecules, and also due to the fact that the muon sticking coefficient after fusion in that molecule is lower, therefore the $dt\mu$ molecule formation possesses special significance. It is after colliding with D_2 and DT molecules that the $dt\mu$ molecule can be formed. However, after the collision of $t\mu$ atom with either of these molecules, there also exists the probability of spin-flip elastic collision. Therefore, in the event that the cross-sections of these collisions $(\sigma_{sf}, \sigma_{el}, \sigma_{mol})$ are available, the probability of molecule formation can be computed via the relation:

$$P_{mol} = \frac{\sigma_{mol}}{\sigma_{mol} + \sigma_{el} + \sigma_{sf}}. \tag{13}$$

Similarly, creating a random number (r_4) and comparing it with P_{mol}, one can determine whether the molecule is formed or not. If $r_4 \le P_{mol}$, the $dt\mu$ molecule will form. In this case, the probability of a fusion in this molecule is certain and after each molecule formation, one can add one number to the number of fusions. Similarly, if $r_4 > P_{mol}$, the probability of elastic collision and, or, spin-flip is computable.

Collision cross-sections depend on the collision energy; therefore, at each stage through which the muonic atom passes, depending on the type of collision it

experiences, the after collision energy must be determined so that in the next collision the related cross-section can be considered.

A $t\mu$ atom, while colliding with hydrogen isotopes can be dispersed in two ways:

(1) The dispersion can be an elastic one in which the total kinetic energy of particles does not change before and after collision. Also, the relative velocity values must be identical before and after collision.

(2) There is the probability of non-elastic dispersion's occurrence as a result of the type of change in the muonic atom's ultra-small structure-, in this case the energy change generated by ultra-small effects, ΔE_{hfs}, has an effect on the projectile particles kinetic energy and the relative velocity after collision:

$$E_{t\mu} + E_{BC} = E'_{t\mu} + E'_{BC} + \Delta E_{hfs}, \tag{14}$$

$$\left|\overrightarrow{V'_{rel}}\right| = \left|\overrightarrow{V_{rel}}\right| \sqrt{1 + \frac{\Delta E_{hfs}}{E}} \tag{15}$$

in which E is the relative kinetic energy before collision, $\overrightarrow{V_{rel}}$ and $\overrightarrow{V'_{rel}}$ are the relative velocity before and after collision, and BC is the type of molecule collided with.

Transition from the ultra-small ground state to the excited one requires energy, the value of which equals the difference in levels in the above mentioned states, ΔE_{hfs}. For the $t\mu$ atom, $\Delta E_{hfs} \approx 240\,\text{meV}$ [18]. It is worth noting that only collision kinetic energy can provide this energy. As a result, for collisions which possess kinetic energy of lesser than $240\,\text{meV}$, transition to ultra-small excited state is, practically, impossible. The cross-section of this process, too, shows an energy threshold in this area [15-17].

A change in the muonic atom's momentum, after collision, depends principally on the angle between the muonic atom's movement direction and the joining axis of two molecular nuclei. To find the muonic atom's momentum, one has to transit the problem to the mass center coordinate system. In case there exists an elastic collision, the relative velocity before and after collision will be the same. It is well known that the molecule targets can be assumed as an imaginary dot mass, the velocity of which equals the velocity of molecule; however, it has a mass tensor which depends on the

molecule structure. For a two-atom *BC* molecule, the target effective mass is [5]:

$$m_B^{eff} = \frac{m_B + m_C}{1 + \frac{m_C}{m_B}\sin^2\beta}, \tag{16}$$

m_B and m_C are the atom's real masses in the *BC* molecule, which are considered to be the $t\mu$ atom's major collision with *B*. β is the average angle between the joining axis of the two nuclei and also the projectile velocity direction *A* at the time of collision. It can be shown that the ultimate velocity of *A* and *B* particles are [5]:

$$\overrightarrow{V_A'} = \overrightarrow{V_{cm}} + \gamma_B \overrightarrow{V_{rel}'}, \tag{17a}$$

$$\overrightarrow{V_B'} = \overrightarrow{V_{cm}} - \gamma_A \overrightarrow{V_{rel}'} \tag{17b}$$

in which:

$$\gamma_B = \frac{m_B^{eff}}{m_A + m_B^{eff}}, \qquad \gamma_A = \frac{m_A}{m_A + m_B^{eff}} \tag{18}$$

and $\overrightarrow{V_{cm}}$ is the mass center velocity vector. Therefore, with the above-mentioned information, one can compute a single particle's ultimate velocity, by choosing random states, with the following procedure:

(1) The first stage deals with determination of the type of molecule colliding with the muonic atom. Also, a nucleus of the above-mentioned molecule which has a leading role in the dispersion must be identified. This nucleus is determined by random selection of the hydrogen isotopes proportional to the percentage of a particular isotope.

(2) One can randomly determine the initial energy and intensity of the molecule present in the medium considering the medium's particles energy distribution function, $f(E, T)$.

The probability of placing particle energy in $[0, E_0]$ is equaled to the random number ξ, which E_0 can be evaluated via the following expressions:

$$\xi = \int_0^{E_0} f(E, T)dE = F(E_0), \tag{19}$$

$$E_0 = F^{-1}(\xi). \tag{20}$$

In case the collision is non-elastic, in addition to a change in the spin direction, the energy after $t\mu$ atom collision is calculated by using computations based on equations (14) and (15). Implicit in this computation is the fact that the total energy after collision in the case when atom spin is transited from $F = 1$ to $F = 0$ increases as much as $0.24\,\text{eV}$.

Subsequently the $t\mu$ atom, for computing the next collision, reaches to its own state of determining the type of molecule subject to collision. This process continues until the muon decays or the $t\mu$ atom, in one of its collisions, is successful in forming a $dt\mu$ molecule and, also, the muon, after fusion in the molecule, sticks to the fusion resulted charged particle. Obviously, each time these processes are repeated, the muon trajectory is numerically computed in different directions, which is, of course, due to the statistical nature of the problem. For each step through which the muon or the muonic atom progresses (based on the type of collision which the program determines which in turn is based on comparing the random number with the cross-sections, using the reaction rate), the time expended in that collision is computed. The time between the two collisions depends on the collision energy and must be computed.

In each stage, the program determines the exact time stage and the amount of energy of the muonic atom. The details of the energy determination and the time computations are explained in the next section. Owing to the fact that muon is an unstable particle with a decay constant of $\lambda_0 = 4.545 \times 10^5 \text{s}^{-1}$, it must be checked periodically for decay. Therefore, statistically, at first a life time is assumed for each muon, $\tau = -\frac{1}{\lambda_0} \text{Ln}\, \xi$, in which ξ is a random number between zero and one. Then, after each collision using the time computation, the first calculation to be checked is a comparison of the spent, with the muon's lifetime. If $t \le \tau$, the muon continues its life; otherwise, it decays and vanishes. This process, for each muon, continues to the point that the muon reaches the stage in the numerical code which is associated with decay or sticking. At this stage in the computations, the Monte-Carlo code selects another entrance muon and this algorithm is re-executed. For each muon that starts a computation, at the time when it vanishes, important quantities such as the number of fusions or the spent time are recorded. The code then continues until the determined

number for the muons is finished. At this stage, the average number of the assumed quantities is recorded and the program repeats for another isotopic concentration.

4. Computing the Cycle Rate, Total Sticking Coefficient, and Fusion Yield Using the Monte-Carlo Method

The code developed for simulating the current problem is based on the Monte-Carlo method. This technique enables the computation of important quantities like the number of catalyzed fusions for one muon which is called the fusion yield and is shown by χ, cycle rate λ_c, and the total sticking coefficient W. The computation of these quantities using the Monte-Carlo method is performed for the first time.

4.1. The cycle rate computation

To achieve this, for each step through which the muon or the muonic atom progresses, based on the type of collision which the program determines (which is based on comparing the random number with the cross-sections, using the reaction rate), the time spent in that collision is computed. The frequent time between the two collisions depends on the collision energy and must be computed. The probability density function for a collision in time t equals:

$$f(t) = \lambda e^{-\lambda t} \tag{21}$$

in which λ is the collision rate and is available from references [1, 13] for molecule formation. In addition, for other collisions, λ, based on the following equation arrives from the cross-sections:

$$\lambda_{ij}^{BC} = NV_{rel}\sigma_{ij}^{BC} \tag{22}$$

in which N is the medium density, V_{rel} is the relative velocity before collision, and σ_{ij}^{BC} is the collision cross-section with BC molecule. C and B can replace either of the hydrogen isotopes. Also, i, j are the muonic atom's spin before and after collision so that in the elastic collision, $i = j$.

The total probability distribution function $F(T)$ is reached using the following equation:

$$F(T) = \int_0^T \lambda e^{-\lambda t} dt = 1 - e^{-\lambda T}. \tag{23}$$

Therefore, the average time between the two collisions can be determined by creating a random number ξ between zero and one:

$$T = -\frac{1}{\lambda} \operatorname{Ln} \xi. \tag{24}$$

By summing up the passed times in the chain of processes which occur in sequence, one after another, the program determines the exact time which the user has reached. Therefore, the time of the first muonic molecule's formation and fusion which takes place at a determinable time during the muon's cycle, is computed. By repeating these computations for many entrance muons (n), and after averaging, the mean time of passing the cycle is computed:

$$\bar{t} = \frac{\sum_t t_i}{n} \tag{25}$$

and then the cycle rate, $\lambda = \frac{1}{\bar{t}}$, is computed.

These computations continue for different hydrogen isotope concentrations, the results of which are shown graphically in Figure 1.

A popular method, repeatedly referred to in many articles, is the use of an equation which gives a general estimation of the cycle rate [1, 2]. Therefore, the longest muon stop time in the cycle can be the muon transition from the $d\mu$ ground state to the $t\mu(\tau_d)$ ground state and forming the $dt\mu$ molecule as a result of a collision between $t\mu$ atoms with D_2 or $DT(\tau_t)$ molecules so that the cycle passing average time can be estimated as follows:

$$\tau = \tau_d + \tau_t = \frac{q_{1s} c_d}{\lambda_{dt} \phi c_t} + \frac{1}{\lambda_{dt\mu} \phi c_d} \tag{26}$$

in which λ_{dt} is the muon transition rate from deuterium to tritium in the ground state and $\lambda_{dt\mu}$ is the $dt\mu$ molecule formation rate. Therefore, we have:

$$\lambda_c^{-1} = \frac{q_{1s} c_d}{\lambda_{dt} \phi c_t} + \frac{1}{\lambda_{dt\mu} \phi c_d}. \tag{27}$$

By employing values for q_{1s}, λ_{dt}, and $\lambda_{dt\mu}$ from references [1, 7, 19] in the

medium with the liquid hydrogen density $(\phi = 1)$, the results, using this equation, are compared in Figure 1. Although the two methods possess the same largeness order λ_c, it is observed that the cycle rate functionality to c_t using the Monte-Carlo method is different. Owing to the fact that in the Monte-Carlo method all collision details, energy functionality, and their spins are considered, it is expected that the results are closer to actual behaviour. Comparing with experimental results adds great credence to the Monte-Carlo model simulations. In Figure 2, the Monte-Carlo computation results are compared with the experimental results for λ_c in $\phi = 0.5$ and $T = 800\,\mathrm{K}$ [20]. This comparison shows that the present computations correlate closely with experimental results. Practically, to reach this temperature and density, high pressures (about 1500 bar) are needed. These conditions are realizable in modern laboratories [20].

Figure 1 shows a comparison between the Monte-Carlo simulation results with equation (27) and the conditions, $T = 1000\,\mathrm{K}$ and $\phi = I$. It is observed that, based on equation (27), that the λ_c value, almost linearly depends on ϕ (of course the q_{1s} value depends on ϕ, but, as Figure 1 shows, the dependence effect of λ_c to ϕ is more of a linear form). However, the Monte-Carlo computations show that figure λ_c can be different from c_t on the basis of the ϕ value. In fact, the collision processes in the medium have fundamental roles in the μCF cycle which are non-linear functions of ϕ and are considered with the Monte-Carlo simulation with precision.

4.2. The total sticking coefficient computation

A muon drops out of the muon catalyzed fusion cycle by sticking to the fusion-resulted charged products in the $dt\mu$, $dd\mu$, and $tt\mu$ molecules. The probabilities of the effective sticking after fusion in the above-mentioned molecules are $w_s = 0.43\%$, $w_{dd} = 12\%$, and $w_{tt} = 14\%$ [2, 17], respectively. Furthermore in the literature, a general estimation of this coefficient is offered using the following equation [21]:

$$W = w_s + \frac{q_{1s} c_d}{\lambda_{dt} c_t + \lambda_{dd\mu} c_d} \left(0.58 \lambda_{dd\mu} c_d w_{dd}\right) + \frac{\lambda_{tt\mu} c_t w_{tt}}{\lambda_{dt\mu} c_d}. \tag{28}$$

This equation is, actually, obtained via the combination of the stickings in different canals, and the formation of $dt\mu$, $dd\mu$, and $tt\mu$ molecules, based on the

statistical share of each canal in the whole cycle [22-31]. In this article, for the first time, the sticking coefficient is computed using the Monte-Carlo computation. To do this, the events which happen to the muonic atoms up to the time of molecule formation are pursued. This is in case after the occurrence of fusion in each molecule formation canals of $dt\mu$, $dd\mu$, and $tt\mu$, the muon sticks to the fusion-resulted charged particle, in which case, one number is added to the counter entered in the Monte-Carlo code in each of the above-mentioned canals. The program is run for many entrance muons $(10^6$ muons). As such the ratio of total number of sticking muons to the total number of the entrance muons will result in the total sticking coefficient. It is worth noting that since there is the probability of the muons becoming free again after fusion and continuing the numerical computations in another route, finally, in one of these roots, the muon sticks to the charged particle and, in this case, the sticking will arrive as one or near to that. To avoid this problem, the muon is allowed to pass the molecule formation stage, in the program, only once, and after the first molecule formation, it performs the next entrance muon computation.

Our computations, based on the Monte-Carlo method, in different tritium concentrations, are shown in Figure 3 and compared with the results of equation (28). It is observed that equation (28), unlike equation (27), possesses an acceptable precision. Of course, for boundary conditions where c_d or c_t are very small, this equation is invalid. However, the Monte-Carlo method simulation results, as we expect, give $W \approx w_{tt} = 14\%$ and $W \approx w_{dd} = 12\%$ for large c_ts and c_ds, respectively.

4.3. The fusion yield computation

The number of the catalyzed fusions for each muon, and the fusion yield, is, also, computed using the Monte-Carlo method. To do this, the events which happen at the time of the muon arrival to the D/T mixture for muons and muonic atoms are pursued, as explained in the previous sections, using the Monte-Carlo method. When, in this route, one reaches a point at which $dt\mu$, $dd\mu$, and, or $tt\mu$ molecules are formed, subsequently fusion is realized. At this point one number is added to the fusions number counter. Then, the muon either sticks to the fusion-resulted charged particle (α) and the program finishes for that muon and the new muon starts its process, or the muon becomes free and repeats the program in another route. During

these processes, the muon may decay, as explained earlier; therefore, when the muon enters the medium so that it can stick to a particle α or decay, the number of fusions for each muon is recorded by the counter. Of course, this quantity must be repeated for many entrance muons and the process of averaging must be done for the achieved results for each muon compared to the number of the entrance muons. The program is done for one million entrance muons and is repeated for different tritium concentrations conditions. The results are illustrated in Figure 4.

The computations related to the fusion yield which have been conducted for the first time, using the Monte-Carlo method are compared with the results of other methods. One of these methods is the cinematic equations solution.

One must note that the super-heating $t\mu$ atoms, while heating, can form $dt\mu$ molecules with more rates, which is ignored in the cycle cinematic solution. Of course, one way to enter the super-heating effects in the cycle cinematic solution is via the parameter η. This is an intrinsic part of super-heating $t\mu$ atoms which, before reaching the heating energy, form the $dt\mu$ molecule. With the implementation of the parameter η in the cycle cinematic equations a greater part of the μCF cycle is completed. However, it seems that computing this quantity does attain sufficient precision. Since the super-heating muonic atoms, in the medium, are produced with different energies, the probability of $dt\mu$ molecule super-heating formation is not equal for all of the super-heating muonic atoms.

In each case, entering the parameter, η, the super-heating muonic atoms effect, on the average, is incorporated into equations. In addition, in the remaining cycle chain processes, the average reaction rate is used. Therefore, for computing important quantities like the number of fusions for one muon, the cycle cinematic solution method, in equilibrium, is not completely precise.

An alternative method is to apply an equation which, based on the concept of fusion yield, gives a general estimation of χ and is usually referred to in many articles [2]. It is defined as follows:

$$\chi = \left(\frac{\lambda_0}{\lambda_c} + W \right)^{-1} \tag{29}$$

in which λ_0 is the muon decay constant W is the total sticking coefficient (equation (28)), and λ_c is the cycle rate (equation (27)).

Figure 4 compares the results related to different methods for computing χ using the Monte-Carlo method. As expected, owning to the fact that the super-heating atoms possess more $dt\mu$ molecule formation cross-section, they increase the yield amount compared to the time they are ignored. However, it is observed that the Monte-Carlo-resulted fusion yield amounts fall between the cycle cinematic-resulted amounts, with and without super-heating effects, respectively, which can be explained as follows. In the computation of η in [22-31], the energy of super-heating $t\mu$ atoms is considered as approximately $60\,\text{eV}$ corresponding to a rise in the values of calculated η. However, practically, superheating $t\mu$ atoms do not possess the same energy and settle in an energy spectrum [9]. Hence, the values of fusion yield in computations of cinematic solution with consideration of the super-heating effects in [22-31] are in excess of the computed value in the present Monte-Carlo computations.

It is worth noting that in the case of high tritium concentration, simulation values attain values close to those obtained by equation (27) and the cinematic solution results. In the next section, it will be shown that in high tritium concentrations, the number of elastic collisions of $t\mu$ atoms increases. Increasing the number of elastic collisions means increasing the $t\mu$ atoms heating velocity. Also, in high tritium values, the number of muon transitions and the super-heating $t\mu$ atoms production both decrease. In other words, super-heating effects in high tritium concentrations are small and the results, in the thermal equilibrium state, can be good. In other tritium concentration values, considering the fact that the Monte-Carlo method is more precise and, also, deals with the collisions details in computations, χ values are computed with greater accuracy.

5. The Fusion Neutrons' Time Spectrum and the Muonic Atoms' Collisions

When a flow from the muons enters the D/T medium and the μCF cycle starts, it is apparent that the fusion-resulted neutrons in the $dt\mu$ molecules do not exit the medium at the same time. The muons enter the medium with a delay; in addition, the statistical nature of the collisions in the μCF cycle causes the creation of the $dt\mu$ muonic molecules at different times following the muons' entrance to the medium. By using Monte-Carlo simulation and determining the time parameter during the process of simulation, the time spectrum of neutrons resulting from fusion is achieved

for one muon (Figure 5). To do this, by dividing the time into small steps $(\Delta t \approx 2\,ns)$ and using concepts discussed in Subsection 4.1 relating to time determination, for each entrance muon, the place of the route termination in the time step is determined (muonic molecule formation) and, also, one is added to that time step's counter. Of course, the muon, after becoming free and repeating the simulation route, forms a $dt\mu$ molecule in another time step. This algorithm is repeated for 10^6 muons and the results of each step are averaged.

In addition, the muon decay diagram $(e^{-\lambda t})$ is shown in Figure 5 beside the time spectrum of fusion neutrons. It is observed that the velocity of the neutrons number moderation for each muon is greater than the muon decay velocity. Therefore, other factors must be involved in moderating the number of neutrons produced, to time. This difference can be related to the medium effect. The most important factor is the muons sticking quality. Therefore, for the sake of a better illustration, the time spectrum for the produced neutrons is provided in Figure 5, neglecting muon decay in program. However, contrary to is expected, except for a marginal elevation in the number of neutrons, this procedure is not particularly effective. The major cause for this is the muon sticking quality which, with the passage of time and cycle repetition by the muon, results in a rise in sticking probability so that up to approximately the first $1\mu s$, most of the muons are eliminated through sticking. This shows that the role of sticking in yield moderation is much more significant than the role of the muon decay. This is one of the advantages of the current simulation, which can assist in computing the results of experiments such as muon decay elimination, which cannot be easily achieved experimentally.

Figure 6 shows the neutrons' time spectrum for different tritium concentrations. The information related to neutrons' time spectrum for the experimental researcher working in neutrons detection, is a good guide. In addition, with a similar method, the time distribution of elastic and non-elastic collisions and, also, muon transition for the muonic atoms $d\mu$ and $t\mu$ in different spin states and different concentrations of tritium are computed. Some of these results are presented in Figures 7 and 8.

6. Energy Spectrum Determination for the Muonic Atoms

As mentioned in Section 2, the muonic atoms are highly excited during their

process of formation which transits to lower states during the cascade processes. During these processes, a muon, in excited states, can be transited from a lighter isotope to a heavier one. The two important collision processes, the Coulombic transitions and the muon transition bring about super-heating muonic atoms. Also, the elastic collisions cause the moderation of the muonic atoms and the muonic atoms energy distribution, in the ground state, depends on these processes [9, 10]. In each case, one of the approximations which can be assumed for the muonic atoms initial distribution, in the ground state, is the Maxwellian distribution, which is used in this article [6]. In this simulation, based on the Maxwellian energy distribution, the muonic atoms initial energy, in the ground state, is determined. Subsequently with Monte-Carlo simulation, the events which happen in the muonic atoms collisions are pursued. If the collision is of the muonic transition type, this causes the production of energetic atoms (equation (4)) and, in the case of an elastic collision it causes the energy moderation of muonic atoms. Also, the spin-flip collisions bring about an energy increase. Therefore, at each instant, the muonic atom's energy changes, and, in each stage, based on what has been elucidated in Sections 3 and 4, the time and energy of the muonic atom, after collision, is recorded. This continues until the decay time of the muon and repeats with the next muon, and so on. In each time step $(\Delta t = 10\,\text{ns})$, the muonic atoms, which are placed in different energy steps, $(\Delta E = 10\,\text{meV})$ are counted. Actually, for each muonic atom with a determined spin, one two-dimensional array is considered, the dimensions of which are energy and time steps. At the end, the entrance muons number to the program is averaged. Therefore, in each time step, the muonic atoms energy spectrum is computed. In other words, due to the time dependence considered in the collisions simulation, one can obtain the energy spectrum time evolution of the muonic atoms. Figures 9 and 10 show the muonic atoms energy spectrum time changes for $c_t = 0.4$.

To better illustrate the energy spectrum, a two-dimensional visualization of the spectrum is given at $t = 150 \pm 1\,\text{ns}$ in Figures 11 and 12. It is observed that the energy spectrum, which was, at first, assumed to be Maxwellian, almost remains the same. As can be seen, the energy spectrum of $t\mu$ atoms is close to the Maxwellian spectrum in the medium temperature $(T = 1000\,\text{K})$. However, it tends toward the moderated energy amounts. This is attributable to super-heating effects and $dt\mu$ molecule formation with higher rate by the super-heating $t\mu$ atoms, which leads to a moderation of the number of $t\mu$ in energies in which the rate of molecule formation

reaches a peak $(0.5\,\text{eV}$ to $E \sim 0.1)$. Also, it is observed in Figure 12 that the $d\mu$ atoms with $\frac{1}{2}$ and $\frac{3}{2}$ spins, to some extent, depart from the Maxwellian distribution toward moderated energies. Actually, in energies between $0.1\,\text{eV}$ to $0.5\,\text{eV}$, the rate of the cross-sections shows that the probability of muon transition from $d\mu$ to tritium is more than for other processes [13]. Therefore, the population of $d\mu$ atoms in these energies is moderated so that their distribution function tends toward lesser energies.

It is worth noting that even if the initial energy spectrum of the muonic atoms, in the ground state, is not Maxwellian, in a short time, it will approach the Maxwellian state. For instance, the energy spectrum which is offered for the muonic atoms (Figure 13) in [9] was considered in the computations and it was shown that, after some nanoseconds, the results converge toward the Maxwellian spectrum. The results, in these conditions, are offered in Figures 14 and 15. In other words, the super-heating effects are important in the first nanoseconds and, then, after the muonic atoms' becoming heated, they lose their influence.

7. Conclusion

In this article, the reactions cycle of the muonic catalyzed fusion is simulated using the Monte-Carlo method, based on a newly-developed numerical code, programmed in FORTRAN. The code includes a time parameter. Therefore, the time spectrum for different events arising in the μCF cycle is reached. In other words, the number of chain events in the μCF cycle, in each time interval, is determined. Also, the fusion-resulted neutrons time spectrum has been achieved. The muonic atoms' energy spectrum was, also, computed in different times and illustrated graphically. Owing to the fact that in the present investigation, at each stage, the muonic atom's energy was computed and the collision processes cross-sections, were used, the precision of the computations is significantly greater than that attained with alternate numerical simulations. The results of the present work were compared to some experimental results and previous computational techniques. A number of important deductions have been made form the current computations. It has been shown that, using equation (27), just an initial estimation of the cycle rate arrives and the dependence of this on the medium density ϕ is more complex than equation (27). The Monte-Carlo results show that in large densities, the graph of λ_c tends toward smaller c_t values so that in $\phi = 1$ and $c_t = 0.4$, the amount of computed λ_c, using

the Monte-Carlo method, shows an effective increase of about 65% compared with the result of equation (27) (Figure 1). The μCF cycle analysis based on cinematic solution methods, which does not consider accurately energy dependence in the collision processes, is different from the Monte-Carlo method results (Figure 4). In high concentrations of tritium, this difference is minimized since the number of elastic collisions of $t\mu$ atoms, compared to other collisions, is greater (Figure 7). In addition, for high values of tritium, the number of muon transitions from $d\mu$ to tritium and energetic $t\mu$ atoms production, is reduced (Figure 8). In other words, the super-heating effects in high concentrations of tritium can be ignored and the results, in the thermal equilibrium state, retain good accuracy.

The Monte-Carlo method in tritium concentrations of between [0.2-0.8] shows that there are no dramatic changes for the fusion yield (Figure 4). Therefore, for the sake of reaching an optimized yield, there is no need for a high concentration of tritium and it is suggested that for the sake of conserving tritium (it is a rare radioactive material), low concentrations of tritium $(c_t \approx 0.3)$ be used.

The fusion-resulted neutrons' time spectrum, the muonic atoms' energy spectrum and also their time evolution, has been efficiently computed using the Monte-Carlo method and analyzed in Sections 5 and 6. We emphasize that without Monte Carlo simulation, this information and the graphs related to the average number of the muonic atoms' different collisions (e.g., the elastic collisions and the muon isotopic transition, as shown in Figures 7 and 8), cannot be computed. It has been shown that the role of muon sticking in moderating the yield is considerably greater than that of muon decay (Figure 5).

It has also been observed that super-heating effects are important in just the first nanoseconds and, also, the muonic atoms' energy spectrum, quickly, tends to the Maxwellian spectrum. Of course, the energy spectrum, to some extent, tends toward the low energies due to the super-heating muonic atoms' consumption in the $dt\mu$ molecule formation which decreases the amount of the muonic atoms in this energy zone of the medium. In case of the $d\mu$ atoms' energy spectrum we highlight that owing to the ratio of the cross-sections in this energy zone, the probability of isotopic transition is greater. Therefore, the $d\mu$ energy spectrum, also tends toward the lower energy amounts. It is worth noting that the data related to the neutrons' time spectrum is a useful guide for the experimental physicist in detecting fusion neutrons.

Acknowledgement

The work described in this paper was fully supported by grants from the Institute for Advanced Studies of Iran. The authors would like to express genuinely and sincerely thanks and their gratitude to Institute for Advanced Studies of Iran.

References

[1] P. Froelich, Muon catalysed fusion chemical confinement of nuclei within the muonic molecule $dt\mu$, Adv. Phys. 41 (1992), 405-508.

[2] C. Petitjean, Progress in muon catalyzed fusion, Nucl. Phys. A 543 (1992), 79-97.

[3] P. Ackerbauer, J. Werner, W. H. Breunlich, M. Cargnelli, S. Fussy, M. Jeitler, P. Kammel, J. Marton, A. Scrinzi, J. Zmeskal, J. Bistirlich, K. M. Crowe, J. Kurck, C. Petitjean, R. H. Sherman, H. Bossy, H. Daniel, F. J. Hartmann, W. Neumann, G. Schmidt and M. P. Faifman, Experimental investigation of muon-catalyzed dt fusion at cryogenic temperatures, Nucl. Phys. A 652 (1999), 311-338.

[4] E. Goldfain, Nonlinear behavior of the renormalization group flow and standard model parameters, Commun. Nonlinear Sci. Numer. Simulat. 12 (2007), 1146-1152.

[5] J. S. Cohen, Thermalization of the muonic tritium atom in deuterium-tritium mixtures, Phys. Rev. A 34 (1986), 2719-2730.

[6] M. Jeitler, W. H. Breunlich, M. Cargnelli, P. Kammel, J. Marton, N. Nägele, P. Pawlek, A. Scrinzi, J. Werner, J. Zmeskal, H. Bossy, H. Daniel, F. J. Hartmann, G. Schmidt, T. von Egidy, C. Petitjean, J. Bistirlich, K. M. Crowe, M. Justice, J. Kurck, R. H. Sherman, W. Neumann and M. P. Faifman, Epithermal effects in muon-catalyzed dt fusion: Comparison of experimental data with theoretical calculations, Phys. Rev. A 51 (1995), 2881-2898.

[7] M. P. Faifman and L. I. Ponomarev, Resonant formation of $dt\mu$ mesic molecules in the triple $H_2 + D_2 + T_2$ mixture, Phys. Lett. B 265 (1991), 201-206.

[8] E. Ding and Y. Huang, Monte Carlo simulation of SATs in 2D, Commun. Nonlinear Sci. Numer. Simulat. 1 (1996), 21-27.

[9] V. E. Markushin, Atomic cascade in muonic hydrogen and the problem of kinetic energy distribution in the ground state, Phys. Rev. A 50 (1994), 1137-1143.

[10] V. E. Markushin, Cascade in muonic and pionic atoms with $Z = 1$, Hyperfine Interactions 119 (1999), 11-21.

[11] L. N. Bogdanova, V. E. Markushin, V. S. Melezhik and L. I. Ponomarev, Lifetime of the mesic molecule $dt\mu$, J. Exp. Theor. Physics 56 (1982), 931-935.

[12] V. Bystritsky, W. Czaplinski and N. Popov, Dynamics of muonic atom cascade in hydrogen-helium mixtures, Eur. Phys. J. D 5 (1999), 185-191.

[13] M. P. Faifman and L. I. Ponomarev, Resonant formation of $dt\mu$ mesic molecules in the triple $H_2 + D_2 + T_2$ mixture, Phys. Lett. B 265 (1991), 201-206.

[14] A. Adamczak, M. P. Faifman, L. I. Ponomarev, V. I. Korobov, V. S. Melezhik, R. T. Siegel and J. Wozniak, Atlas of cross sections for scattering of muonic hydrogen atoms on hydrogen isotope molecules, Atomic Data and Nuclear Data Tables 62 (1996), 255-344.

[15] J. S. Cohen and M. C. Struensee, Improved adiabatic calculation of muonic-hydrogen atom cross sections. I. Isotopic exchange and elastic scattering in asymmetric collisions, Phys. Rev. A 43 (1991), 3460-3473.

[16] J. S. Cohen, Improved adiabatic calculation of muonic-hydrogen-atom cross sections. II. Hyperfine transitions and elastic scattering in symmetric collisions, Phys. Rev. A 43 (1991), 4668-4683.

[17] J. S. Cohen, Improved adiabatic calculation of muonic-hydrogen-atom cross sections. III. Hyperfine transitions in asymmetric collisions, Phys. Rev. A 44 (1991), 2836- 2845.

[18] L. I. Ponomarev, Muon catalysed fusion, Contemp. Phys. 31 (1990), 219-245.

[19] W. Czapliński, A. Gul/a, A. Kravtsov, A. Mikhailov and N. Popov, Muon transfer in excited muonic hydrogen, Phys. Rev. A 50 (1994), 518-524.

[20] V. R. Bom, J. N. Bradbury, J. D. Davies, A. M. Demin, D. L. Demin, C. W. E. van Eijk, V. V. Filchenkov, A. N. Golubkov, N. N. Grafov, V. G. Grebinnik, S. K. Grishechkin, K. I. Gritsaj, V. G. Klevtsov, A. D. Konin, A. A. Kukolkin, S. V. Medved, V. A. Nazarov, V. V. Perevozchikov, A. N. Ponomarev, V. Ya. Rozhkov, A. I. Rudenko, S. M. Sadetsky, Yu. V. Smirenin, N. I. Voropaev, A. A. Yukhimchuk, S. A. Yukhimchuk, V. G. Zinov and S. V. Zlatoustovskii, Investigation of the parameters of muon-catalyzed fusion in double D/T mixture at high temperature and density, Hyperfine Interactions 138 (2001), 213-223.

[21] S. E. Jones, A. N. Anderson, A. J. Caffrey, C. DeW. Van Siclen, K. D. Watts, J. N. Bradbury, J. S. Cohen, P. A. M. Gram, M. Leon, H. R. Maltrud and M. A. Paciotti, Observation of unexpected density effects in muon-catalyzed d-t fusion, Phys. Rev. Lett. 56 (1986), 588-591.

[22] R. Farnoosh and M. Ebrahimi, Monte Carlo simulation via a numerical algorithm for solving a nonlinear inverse problem, Commun. Nonlinear Sci. Numer. Simulat. 15 (2010), 2436-2444.

[23] M. Kastner, Monte Carlo methods in statistical physics: Mathematical foundations and strategies, Commun. Nonlinear Sci. Numer. Simulat. 15 (2010), 1589-1602.

[24] S. Mitra, A. Mitra and D. Kundu, Genetic algorithm and M-estimator based robust sequential estimation of parameters of nonlinear sinusoidal signals, Commun. Nonlinear Sci. Numer. Simulat. 16 (2011), 2796-2809.

[25] F. Guiaş, A stochastic approach for simulating spatially inhomogeneous coagulation dynamics in the gelation, Commun. Nonlinear Sci. Numer. Simulat. 14 (2009), 204-222.

[26] F. Jiang, Y. Shen and L. Liu, Numerical methods for a class of jump-diffusion systems with random magnitudes, Commun. Nonlinear Sci. Numer. Simulat. 16 (2011), 2720-2729.

[27] D. Yang, Chaos control for numerical instability of first order reliability method, Commun. Nonlinear Sci. Numer. Simulat. 15 (2010), 3131-3141.

[28] J. Feng, W. Zhu and Z. Liu, Stochastic optimal time-delay control of quasi-integrable Hamiltonian systems, Commun. Nonlinear Sci. Numer. Simulat. 16 (2011), 2978-2984.

[29] P. Valkó and X. Zhang, Finite domain anomalous spreading consistent with first and second laws, Commun. Nonlinear Sci. Numer. Simulat. 15 (2010), 3455-3470.

[30] J. Machado, V. Kiryakova and F. Minardi, Recent history of fractional calculus, Commun. Nonlinear Sci. Numer. Simulat. 16 (2011), 1140-1153.

[31] J. Yang, X. Cai and X. Liu, The maximal Lyapunov exponent for a three-dimensional system driven by white noise, Commun. Nonlinear Sci. Numer. Simulat. 15 (2010), 3498-3506.

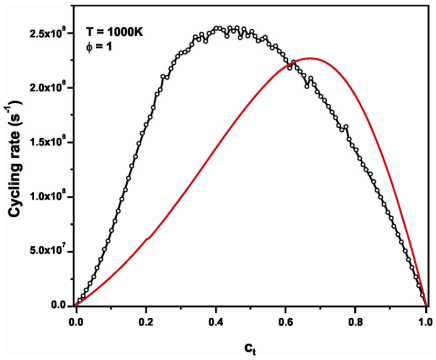

Figure 1. Comparing the achieved cycle rate from the Monte-Carlo method $(\circ)$ with curve equation (27) under conditions $T = 1000\,\mathrm{K}$ and $\phi = 1$.

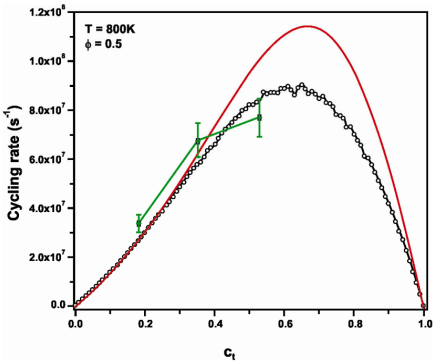

Figure 2. Comparing the achieved cycle rate from the Monte-Carlo method $(\circ)$ and curve equation (27) with experimental results under conditions $T = 800\,\mathrm{K}$ and $\phi = 0.5$.

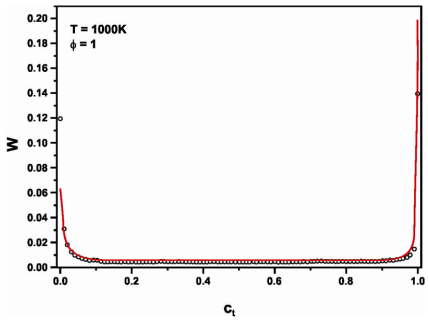

Figure 3. Comparing the total sticking coefficient computed by the Monte-Carlo method $(\circ)$ with curve equation (28) for conditions $T = 1000\,\mathrm{K}$ and $\phi = 1$.

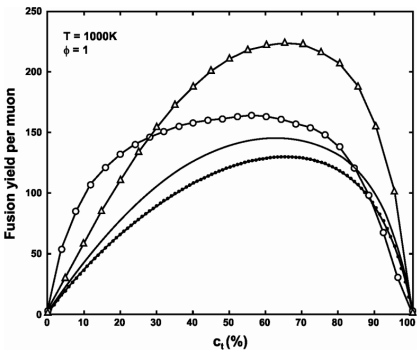

Figure 4. Comparing the fusion number changes graph for each muon with the tritium concentration, from the cinematic solution methods $(\bullet)$, the cinematic solution considering the super-heating atoms effects (Δ), curve equation (29) and the Monte-Carlo simulation $(\circ)$ (present study) with conditions $T = 1000\,\mathrm{K}$ and $\phi = 1$.

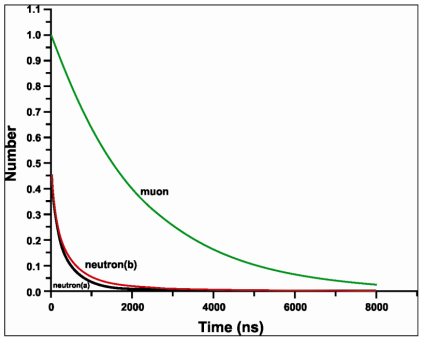

Figure 5. The fusion neutrons' time spectrum with conditions $T = 1000\,\mathrm{K}$, $\phi = 1$, and $c_t = 0.4$ in two states with (a) muon decay and (b) neglecting muon decay and comparison with the muon decay graph.

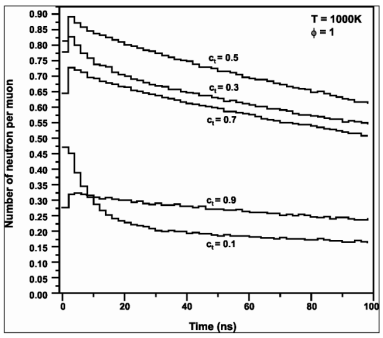

Figure 6. The fusion neutrons' time spectrum for different concentrations of tritium with conditions $T = 1000\,\mathrm{K}$ and $\phi = 1$.

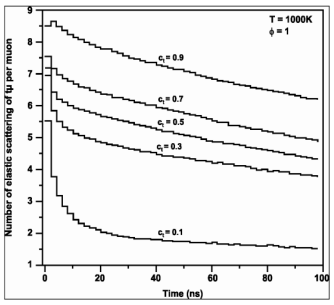

Figure 7. The elastic collisions' time spectrum of $t\mu$ atoms for different concentrations of tritium with conditions $T = 1000\,\mathrm{K}$ and $\phi = 1$.

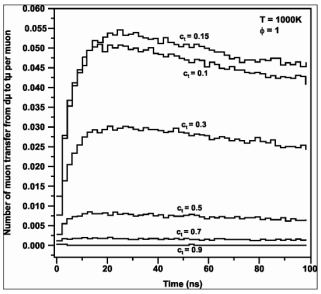

Figure 8. The muon transition time spectrum from $t\mu$ to t for different concentrations of tritium with conditions $T = 1000\,\mathrm{K}$ and $\phi = 1$.

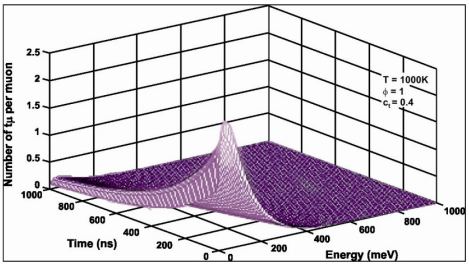

Figure 9. The $t\mu$ muonic atoms' energy spectrum time evolution for conditions $T = 1000\,\mathrm{K}$, $\phi = 1$, and $c_t = 0.4$.

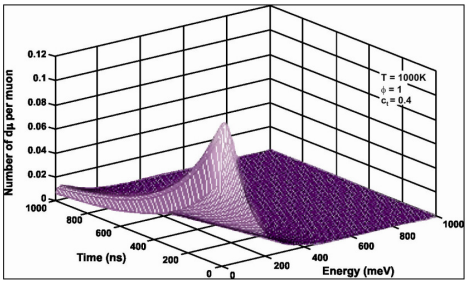

Figure 10. The $d\mu$ muonic atoms' energy spectrum time evolution for conditions $T = 1000\,\mathrm{K}$, $\phi = 1$, and $c_t = 0.4$.

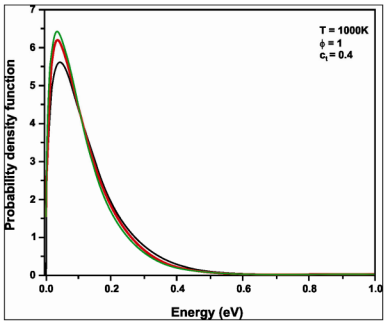

Figure 11. Comparing the $t\mu^0$ and $t\mu^1$ munic atoms' energy spectrum in $t = 150 \pm 1\,\mathrm{ns}$ for conditions $T = 1000\,\mathrm{K}$, $\phi = 1$, and $c_t = 0.4$ using the Maxwellian energy distribution.

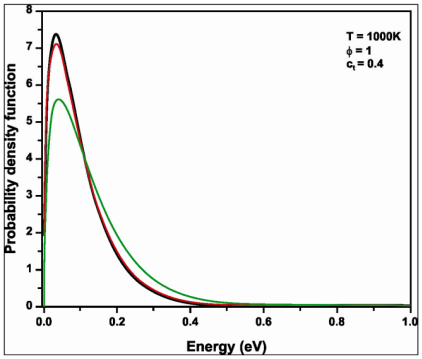

Figure 12. Comparing the $d\mu^{1/2}$ and $d\mu^{3/2}$ in muonic atoms' energy spectrum with $t = 150 \pm 1\,\text{ns}$ for conditions $T = 1000\,\text{K}$, $\phi = 1$, and $c_t = 0.4$ using the Maxwellian energy distribution.

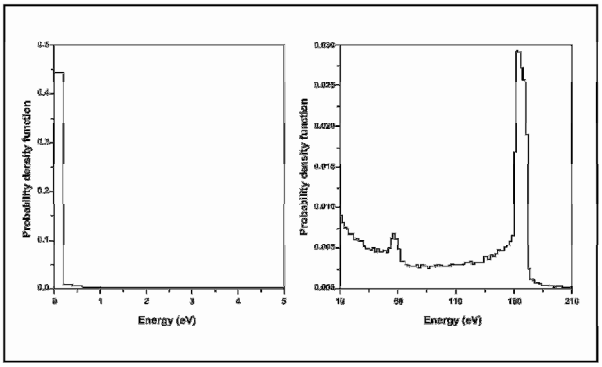

Figure 13. The kinetic energy distribution of muonic atoms in ground state [9].

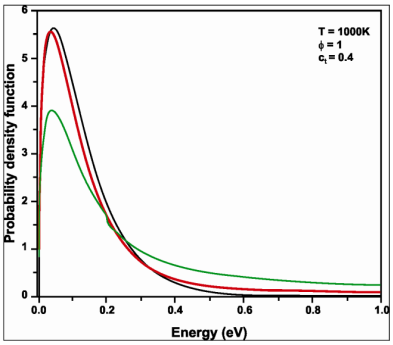

Figure 14. The muonic atoms' energy spectrum $t\mu^0$ and $t\mu^1$ in $t = 150 \pm 1\,\text{ns}$ with $T = 1000\,\text{K}$, $\phi = 1$, and $c_t = 0.4$ conditions and also with the condition that initial

energy of muonic atoms is not the Maxwellian in the ground state and has been substituted from [9] and its comparison with the Maxwellian energy distribution.

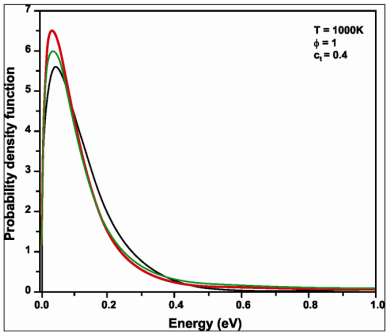

Figure 15. The muonic atoms' energy spectrum $d\mu^{1/2}$ and $d\mu^{3/2}$ in $t = 150 \pm 1$ ns with conditions $T = 1000$ K, $\phi = 1$, and $c_t = 0.4$ and also with conditions that initial energy of muonic atoms is not the Maxwellian in ground state and has been substituted from [9] and its comparison with the Maxwellian energy distribution.